Catalysis Today 143 (2009) 230–236

Contents lists available at ScienceDirect

Catalysis Today

journal homepage: www.elsevier.com/locate/cattod

Synthesis of $Ti_{1-x}Sn_xO_2$ nanosized photocatalysts in reverse microemulsions

Fernando Fresno [a,b,*], David Tudela [b], Juan M. Coronado [c], Javier Soria [a]

[a] Instituto de Catálisis y Petroleoquímica, CSIC, C/Marie Curie 2, Cantoblanco, 28049 Madrid, Spain
[b] Departamento de Química Inorgánica, Facultad de Ciencias, Universidad Autónoma de Madrid, 28049 Madrid, Spain
[c] Aplicaciones Medioambientales de la Energía Solar. CIEMAT, Av. Complutense 22, 28040 Madrid, Spain

ARTICLE INFO

Article history:
Available online 18 December 2008

Keywords:
Photocatalysis
Titania
Sn
Doped
Microemulsion
Trichloroethylene

ABSTRACT

The preparation of $Ti_{1-x}Sn_xO_2$ nanocrystalline photocatalysts in reverse microemulsions is reported in this work. The obtained materials have been characterised by total reflection X-ray fluorescence (TXRF), X-ray diffraction (XRD) and Raman and UV–vis spectroscopies. Very good accordance between calculated and obtained compositions is observed. Undoped TiO_2 prepared in this way crystallises in the anatase phase. Tin-doped anatase is formed with $x < 0.05$, while both anatase and rutile phases crystallise when $x \geq 0.05$. When both phases coexist, a preferential doping of rutile seems to occur. When $x = 0.10$, a multiphase mixture containing TiO_2(anatase), TiO_2(rutile) and SnO_2 was formed. No significant modification of the band gap is found in any case. The photocatalytic activity of the obtained catalysts is compared employing the trichloroethylene photocatalytic degradation as a test reaction. The beneficial effect of Sn^{4+} in the activity of TiO_2 appears to be related to the formation of anatase–rutile mixtures, leading to the highest specific photocatalytic activity in the sample of composition $Ti_{0.93}Sn_{0.07}O_2$, with anatase:rutile ratio close to 3.

© 2008 Elsevier B.V. All rights reserved.

1. Introduction

Among the different semiconductors that have been tested for environmental photocatalytic applications, TiO_2 is by far the most commonly used, because it provides the best compromise between photocatalytic activity and stability in operation conditions, being, in addition, inexpensive and essentially non-toxic [1,2]. Nevertheless, in order to further improve the performance of TiO_2, several chemical and structural modifications of this material have been assayed. Significant improvements in photocatalytic reaction rates have been achieved with the use of nanosized TiO_2 [3], in accordance with what is frequently observed in heterogeneous catalysis [4]. In addition, cationic doping of titania has been widely explored to obtain more active photocatalysts [5,6]. Among the studied dopant cations, several works have reported on the improvement of titania by the incorporation of Sn^{4+} into the TiO_2 lattice, either in the anatase or rutile phase as well as in mixtures of both [7–10]. Different preparation methods have been used for the synthesis of $Ti_{1-x}Sn_xO_2$ materials, including sol–gel methods [11,12], chemical vapour deposition [13,14], co-precipitation [8,15], mechanochemical synthesis [16,17] and, recently, synthetic methods for producing hollow spheres [18,19]. In previous works, we have reported on the preparation of multiphase $Ti_{1-x}Sn_xO_2$ nanoparticles, obtained by means of the reaction between $TiCl_4$ and Ph_3SnOH [20]. The obtained photocatalysts presented in most cases a higher activity than undoped TiO_2 for the photocatalytic oxidation (PCO) of methylcyclohexane and toluene vapours [10,21]. In addition, the use of these catalysts in the photocatalytic degradation of aqueous suspensions of the herbicide chlorsulfuron led to higher degradation rates when Sn^{4+} was doped into TiO_2 [22]. The activity of the tin-doped photocatalysts was considered to be influenced by the anatase to rutile ratio, by the extent of the interphase between crystallites of different phases and by electronic modifications induced by doping [23]. However, the employed synthetic route, although leading to highly active photocatalysts, presented the limitation that the Sn content in the final materials could not be easily modulated.

Microemulsion-mediated syntheses have been widely employed for the preparation of nanocrystalline catalysts [24]. Nanosized TiO_2 [25,26] and doped TiO_2 [27] photocatalysts have been obtained by this technique. In this work, we report on the preparation of $Ti_{1-x}Sn_xO_2$ photocatalysts in reverse microemulsions, with varying concentration of dopant ions. The obtained materials are characterised by TXRF, XRD and Raman and UV–vis spectroscopies. The gas-phase photocatalytic degradation of

* Corresponding author. Present address: Unidad de Sistemas de Concentración Solar. CIEMAT, Avda. Complutense 22, 28040 Madrid. Spain.
E-mail address: fernando.fresno@ciemat.es (F. Fresno).

0920-5861/$ – see front matter © 2008 Elsevier B.V. All rights reserved.
doi:10.1016/j.cattod.2008.10.024

trichloroethlyene (TCE) is used as a model reaction to test the photocatalytic activity of the synthesised materials. To the best of our knowledge, this is the first time that the microemulsion synthesis of tin-doped TiO_2 is reported.

2. Experimental

2.1. Materials

For the synthesis of $Ti_{1-x}Sn_xO_2$ materials, ranging from $x = 0.01$ (TiSnM1) to $x = 0.10$ (TiSnM10), a reverse microemulsion of water in n-heptane (Scharlau), using 1-hexanol (Aldrich) and Triton X-100 (Aldrich) as surfactants, was employed. The water:n-heptane:Triton:1-hexanol volume ratios were 1:8.54:1.77:1.86. To obtain this microemulsion, the adequate amounts of the organic components were mixed and magnetically stirred for 1 h in an Erlenmeyer flask. Then water was added and the mixture was again stirred for 1 h, after which an homogeneous transparent emulsion was obtained. A solution of the appropriate quantities of $Ti(O^iPr)_4$ (Aldrich) and $SnCl_4{\cdot}5H_2O$ (Probus) in ^{i}PrOH (Aldrich) was then added dropwise to the stirred microemulsion, which immediately turned turbid. The mixture was then kept under magnetic stirring for 24 h, after which the solid was separated by centrifugation, rinsed with methanol and dried at 50 °C. The obtained powders were then crystallised by thermal treatment in air at 723 K for 3 h with a temperature ramp of 7 K min^{-1}. A blank TiO_2 sample (TiM) was obtained following the same method except for the absence of $SnCl_4{\cdot}5H_2O$. For the synthesis of TiSnM10, the aqueous phase was composed of a ca. 3.8 M NH_3 solution. This basic medium was employed in order to neutralize the HCl formed from the hydrolysis of $SnCl_4$, as it was observed that, with the amount of $SnCl_4{\cdot}5H_2O$ needed for the desired composition $Ti_{0.90}Sn_{0.10}O_2$, the pH after the reaction was low enough to avoid sedimentation of the final product, probably because of the formation of a stable colloidal solution.

2.2. Characterisation techniques

The tin content of the doped samples was determined by total reflection X-ray fluorescence spectroscopy (TXRF), using a TXRF EXTRA-II Rich & Seifert equipment. Surface areas were calculated, by means of the BET method, from nitrogen adsorption isotherms obtained at 77 K in a Micromeritics Tristar 3000 apparatus, after outgassing the samples at 413 K. Powder X-ray diffraction patterns were recorded on a Seifert XRD 3000P diffractometer using nickel-filtered Cu Kα radiation. The average particle size was calculated by the Scherrer equation from the width of the most intense reflections: (1 0 1) for anatase and (1 1 0) for rutile, and microstrain values were estimated from Williamson–Hall plots [28]. Unit cell parameters a and c, and then unit cell volumes, were calculated by least square fitting of the experimental data to the equation:

$$d^{-2}_{(h\,k\,l)} = (h^2 + k^2)a^{-2} + l^2c^{-2} \quad (1)$$

where $d_{(h\,k\,l)}$ is the distance between the ($h\,k\,l$) crystal planes. Rutile:anatase weight ratios were also estimated from the XRD data [29] by means of Eq. (2):

$$W_R = \frac{A_R}{0.884A_A + A_R} \quad (2)$$

where W_R is the proportion of rutile, and A_A and A_R are the integrated areas of the (1 0 1) peak of anatase and the (1 1 0) peak of rutile, respectively.

Raman spectra were recorded in a Renishow Micro-Raman System 1000 spectrometer, equipped with a charge coupled detector operating at 200 K and a holographic filter to eliminate elastic dispersion. The excitation source was the 633 nm line of a 10 mW powered Ar laser, and 5 scans with 30 s accumulation and 3 cm^{-1} resolution were recorded. UV–vis diffuse reflectance spectra were registered on a Shimadzu UV-2401 PC spectrometer using $BaSO_4$ as a reference. The band gap energies of the different samples were estimated from UV–vis spectra according to the procedure described by Serpone et al. [30].

2.3. Photocatalytic reactions

The gas-phase photocatalytic degradation of trichloroethylene (TCE) was used as a model reaction to test the activities of the obtained photocatalysts. A synthetic air stream (600 sccm) was passed through a bubbler that contained TCE (Panreac, 99%) at 258 K. The saturated gas was conducted to the photoreactor, which consisted of a rectangular cell with Pyrex glass windows externally illuminated by two UV lamps (Philips UVA TL8W05-1). The catalyst (ca. 20 mg) was supported, from an ethanol slurry, on a Pyrex glass slide that was introduced into the reaction cell. The reaction gas passed through the cell over the catalyst layer. The outlet gas flow was analyzed by on-line infrared spectroscopy, with a Nicolet 5700 FTIR spectrometer equipped with a heated (383 K) Thermo-gas cell with BaF_2 windows.

3. Results and discussion

3.1. Characterisation of the photocatalysts

Table 1 shows the tin contents and structural, morphological and electronic characteristics of the different prepared photocatalysts. As it can be observed in the table, the obtained amounts of Sn in the final products are in very good accordance with those

Table 1
Characteristics of the photocatalysts.

Sample	$Ti_{1-x}Sn_xO_2$		S_{BET} (m^2/g)	Crystalline phases	Crystal size (nm)	Microstrain $\Delta d/d$	Cell volume (Å^3)[a]	Indirect band gap (eV)	Direct band gap (eV)
	Calculated x	Obtained x							
TiM	0	0	83	Anatase	9	0.0007	135.8(8)	2.94	3.19
TiSnM1	0.01	0.01	133	Anatase	7	0.0012	135.4(8)	2.94	3.25
TiSnM3	0.03	0.03	147	Anatase	7	0.0013	135.9(8)	3.01	3.26
TiSnM5	0.05	0.05	107	Anatase (85%)	8	0.0011	135.9(8)	2.97	3.25
				Rutile (15%)	10	0.0245	63.8(5)		
TiSnM7	0.07	0.07	101	Anatase (76%)	9	0.0008	136.7(8)	2.95	3.10
				Rutile (24%)	10	0.0119	63.7(5)		
TiSnM10	0.10	0.11	93	Anatase (85%)	8	0.0017	135.6(8)	3.05	3.20
				Rutile (15%)	5	0.0021	63.7(5)		
				SnO_2	6	–	–		

[a] PDF values: 135.9 (anatase), 62.4 (rutile).

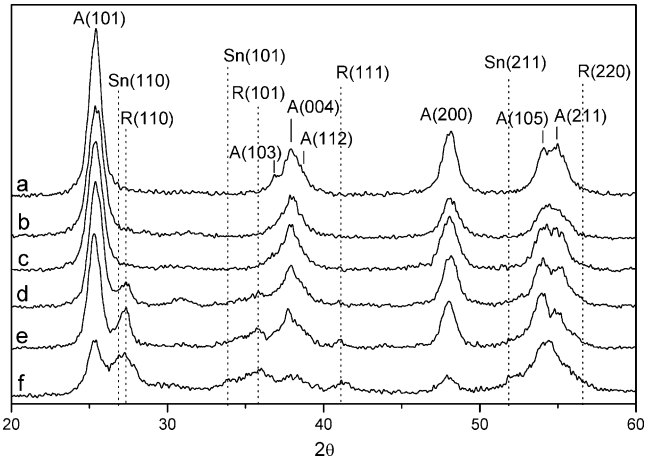

Fig. 1. XRD patterns of the photocatalysts: (a) TiM, (b) TiSnM1, (c) TiSnM3, (d) TiSnM5, (e) TiSnM7, (f) TiSnM10. A: anatase, R: rutile, Sn: SnO_2.

calculated for their syntheses. This indicates that the hydrolysis of $Ti(O^iPr)_4$ and $SnCl_4$ has been completed in the employed reaction conditions. Only a slight deviation of the obtained Sn concentration with respect to the nominal value occurs in the sample containing the highest dopant level, TiSnM10. The addition of NH_3 in the synthesis process of this sample may be related to the slightly increased Sn/Ti ratio. On the other hand, an inversion in the order of addition of metals and base gave rise to a material essentially equal to TiSnM10.

Fig. 1 shows the XRD patterns of the obtained materials. Only diffraction peaks corresponding to the anatase crystalline form of TiO_2 are present in the pattern of the undoped titania sample TiM. This is in accordance with previously reported results for pure TiO_2 at the same calcination temperature [23,31]. Anatase also appears as the only crystalline phase in samples TiSnM1 and TiSnM3. However, with a higher Sn^{4+} loading, the rutile structure begins to form, in addition to anatase, as it can be observed in the diffractogram of TiSnM5, with the appearance of low intensity peaks at 27.25 and ca. 36°. The formation of rutile in conditions under which anatase is the preferred crystalline structure in undoped TiO_2 is the first observable effect of tin doping. This effect was already known, and, indeed, SnO_2 has been employed to favour rutile crystallisation in TiO_2-based ceramic membranes [32,33], and the formation of rutile has been observed in previously reported tin-doped TiO_2 samples obtained by other procedures than the microemulsion method employed here [10,12,34]. Nevertheless, the preparation method plays an important role in the obtained phases and, when the hydrolysing medium contains nitric acid, tin-doped TiO_2 obtained by a sol–gel method is more prone to crystallise in the anatase structure [7]. For example, $Ti_{0.95}Sn_{0.05}O_2$ photocatalysts prepared by Liqiang et al. [35] had the anatase structure after calcination at 500 °C, while TiSnM5, with the same dopant level, has both anatase and rutile, after calcination at only 450 °C, although higher calcination temperatures favour the formation of rutile. With our synthetic procedure, however, it appears that a minimum Sn/Ti ratio is necessary for rutile formation, although the presence of a small amount of this phase, not observable by XRD, cannot be discarded in TiSnM1 and TiSnM3. The proportion of rutile increases in TiSnM7, as estimated from the peak areas and shown in Table 1, indicating that a higher Sn^{4+} content leads to the formation of this phase in a higher proportion. With further increased Sn^{4+} concentration, in sample TiSnM10, a segregated SnO_2 phase with rutile type structure (cassiterite) appears, in addition to anatase and rutile, as demonstrated by the diffraction peaks at ca. 34° and 52°, as well as the shoulder on the high angle side of the (1 1 0) peak of rutile. In the case of TiSnM7, the shoulder on the low-angle side of the (1 0 1) diffraction peak of rutile suggests the presence of a slight amount of very small SnO_2 crystals, although no other diffractions from the cassiterite phase can be envisaged. The formation of SnO_2 in the sample with highest Sn loading suggests that the TiO_2 lattice has exceeded the solubility limit for Sn^{4+} incorporation, although the influence of the addition of NH_3 in the synthesis process cannot be discarded. Regarding the TiO_2 saturation for the accommodation of Sn^{4+}, different results have been reported in the literature. It is generally assumed that for solid solutions $Ti_{1-x}Sn_xO_2$ with rutile structure, only TiO_2-rich ($x < 0.1$) and SnO_2-rich ($x > 0.1$) phases are thermodynamically stable at room temperature [7,36], although metastable solid solutions have often been obtained with intermediate compositions [7]. In this way, Kulshreshtha et al. reported the formation of a single phase in all the composition interval in $Ti_{1-x}Sn_xO_2$ solid solutions with rutile structure, obtained by co-precipitation and calcined at 800 °C [15], while, on the other hand, Lin et al. observed cassiterite segregation in a rutile $Ti_{1-x}Sn_xO_2$ material with $x = 0.10$ prepared by the citric acid complexation method and calcined at 710 °C [8]. Therefore, the preparation method seems to play a key role on the solid solution limits in the TiO_2–SnO_2 system. As far as the solubility of SnO_2 in anatase is concerned, although no studies are available, it is expected to be smaller than in rutile, because Sn seems to concentrate preferentially in rutile when both phases are present [23]. In addition to the mentioned crystalline phases, the diffraction pattern of TiSnM5 shows a wide peak with low intensity at ca. 30.5°, not observed in the rest of samples, which may be caused by a small amount of the brookite phase of TiO_2.

The mean crystal sizes calculated with the Scherrer formula are a few nanometres for all the samples and crystalline phases, thus revealing the effect of the microemulsion synthetic method on crystal growth [24]. Regarding the estimated microstrains, in the case of anatase, the strain values increase in general terms with respect to TiO_2 with the incorporation of Sn. Microstrain has been related, in addition to crystal size effects, to the presence of guest cations in the TiO_2 lattice [37,38]. However, after a first increase in low dopant level anatase samples, a drop in the anatase microstrain is observed when the rutile phase appears and increases its proportion, i.e., from TiSnM3 to TiSnM5 and from TiSnM5 to TiSnM7. A similar trend is found regarding anatase crystal sizes, for which a decrease is generally related to cationic doping of TiO_2 [11,37]. In previous works on tin-doped TiO_2 samples formed by rutile and anatase, a preferential Sn concentration in rutile was proposed [23], and a lower effect of Sn^{4+} in anatase when both phases are present may be related to this preferential doping. In the case of rutile, higher microstrain values are obtained with respect to anatase, which may be considered as an effect of increased Sn^{4+} concentration. The rutile microstrain decreases on going from TiSnM5 to TiSnM7 because, although the total tin amount increases from 5 to 7%, the rutile proportion also increases from 15 to 24% (see Table 1), so that the tin concentration in rutile might decrease. In the case of TiSnM10, the different preparation method and the presence of a SnO_2 phase lead to a different behaviour.

The cell volumes calculated from the XRD data are also shown in Table 1. Regarding the anatase phase, no significant differences are observed between the values obtained for the tin-doped samples and the TiO_2 reference material. In the case of rutile, the value found in the powder diffraction file (PDF) of the ICDD is taken as a reference. This reference may be considered valid, since the comparison of the cell volumes of anatase in the PDF and in TiM reveals no effect of the preparation method on the cell dimensions. The volumes obtained for the rutile phase in TiSnM5, TiSnM7 and TiSnM10 do present a significant increase with respect to the PDF

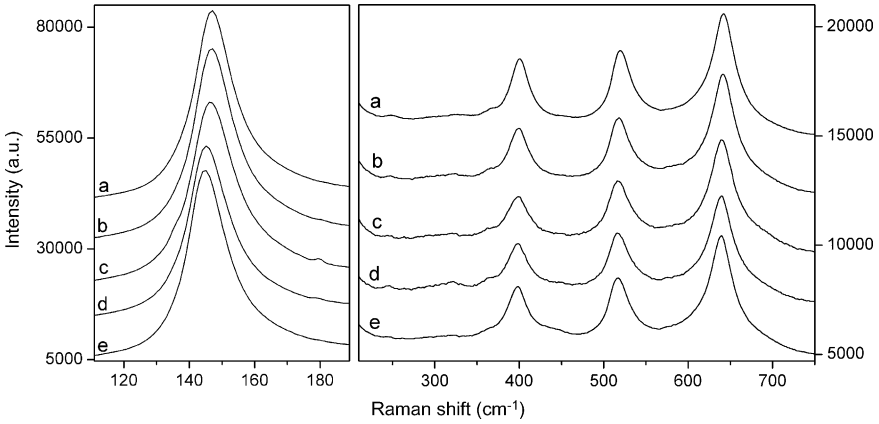

Fig. 2. Raman spectra of (a) TiM, (b) TiSnM1, (c) TiSnM3, (d) TiSnM5, and (e) TiSnM7.

value, taking into account the estimated experimental errors. Therefore, the presence of Sn^{4+} has caused an expansion of the rutile lattice. Furthermore, if we compare the rutile unit cell volumes in TiSnM5 and TiSnM7 with those obtained by Kulshreshtha et al. for $Ti_{1-x}Sn_xO_2$ ($0 \leq x \leq 1$) solid solutions with rutile structure [15], we can see that they are higher than those corresponding to $x = 0.05–0.07$, thus suggesting that the real tin concentration in the rutile phase is higher than that in the whole sample, as suggested by the microstrain values. However, the cell volumes of TiSnM5, TiSnM7 and TiSnM10 are similar, so that no effect of the doping level is observed, which may be related, as noted above, to the simultaneous increase of tin content and rutile proportion, on going from TiSnM5 to TiSnM7, and to the presence of a SnO_2 phase in TiSnM10. With respect to anatase, it is not surprising that no significant volume changes are observed in Table 1, because small changes, as compared to the experimental errors, are expected for a Sn doping level up to 3%, and for higher tin amounts, preferential concentration in rutile reduces its concentration in anatase when both phases are present. Furthermore, the anatase crystal structure is more open than that of rutile, as demonstrated by their respective densities (3830 and 4240 kg m^{-3} for anatase and rutile, respectively), so that it is possible that the cell volume of this phase is less affected by the accommodation of Sn^{4+} ions.

Regarding BET surface areas, the obtained values are in general lower than those estimated from the mean crystal sizes, which suggests a significant agglomeration of crystals into secondary particles. This has been previously observed in microemulsion-prepared TiO_2 samples [25]. However, the trend in S_{BET} is in good agreement with that expected from crystal sizes.

Fig. 2 shows the Raman spectra of the samples with doping levels from 0 to 7 atomic percent. In the 200–700 cm^{-1} range (right part of the figure), bands corresponding to vibrations of the anatase structure are observed, at ca. 399 (B_{1g}), 517 ($A_{1g} + B_{1g}$) and 604 cm^{-1} (E_g) [11,39,40], with precise positions varying slightly in the different samples. In the spectrum of TiSnM5, no signals assigned to rutile can be observed, despite the fact that this phase was detected by XRD. The amount of rutile in this sample (15% as estimated from XRD) may not be high enough for the Raman bands to be clearly detected. In this respect, the signals of rutile in other TiSn samples were observed with very low intensity even with estimated rutile contents of 50% [23]. In TiSnM7, a signal at ca. 443 cm^{-1}, assigned to rutile (E_g) [39,41], is observed as a shoulder of the B_{1g} band of anatase. However, the band of rutile at 609 cm^{-1} (A_{1g}) [39,41] is not detected in any of the rutile containing samples. Probably, this band is totally overlapped by the width of the signal of anatase at 640 cm^{-1}. In addition to the mentioned bands, signals attributable to brookite (245, 321 and 363 cm^{-1}) [42], with low intensity, are observed in some of the samples. It is possible, then, that this phase exists in these samples in a low proportion. Brookite was indeed detected in the XRD study of sample TiSnM5. The appearance of brookite has also been observed in W-doped TiO_2 samples prepared in reverse microemulsions [37]. On the other hand, signals attributable to SnO_2 are not detected in any of these samples [43]. The part of the Raman spectra in which the most intense band of anatase appears (E_g) is represented in the left part of Fig. 2 at a different scale, so that the asymmetric widening and the consequent shift of the maximum caused by the small crystal size [39,44] can be observed. The position and width of this band in the different samples will be discussed below. The spectrum of sample TiSnM10, not shown, presents a different aspect than those in Fig. 2. The intensity of the signals is considerably lower and their width larger, and a rising background is observed. This reveals, together with the XRD pattern, the low crystallinity of this sample. In this Raman spectrum, bands corresponding to anatase are observed, apart from wide signals that may correspond to overlapping bands of both rutile and SnO_2.

The positions and widths of the anatase Raman line at ca. 146 cm^{-1} in the spectra of samples with 0–7% Sn are plotted in Fig. 3 against the reciprocal of crystal size, along with lines representing the values expected from the phonon confinement

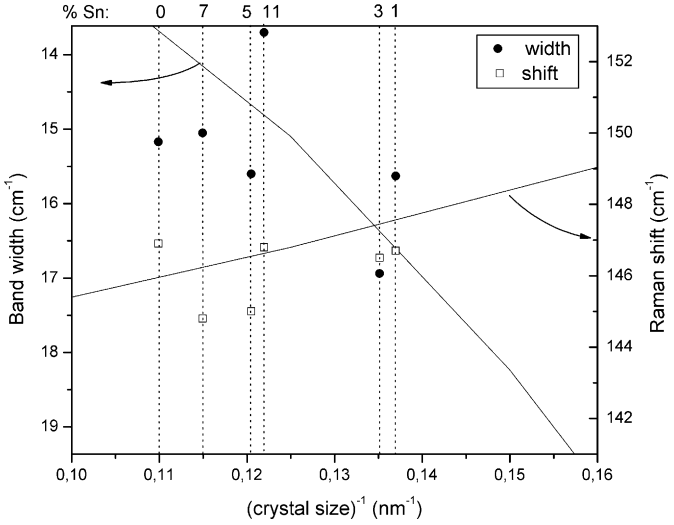

Fig. 3. Variation with crystal size of the full width at half maximum and Raman shift of the 143 cm^{-1} band of anatase. The solid lines represent the expected trends from the phonon confinement model.

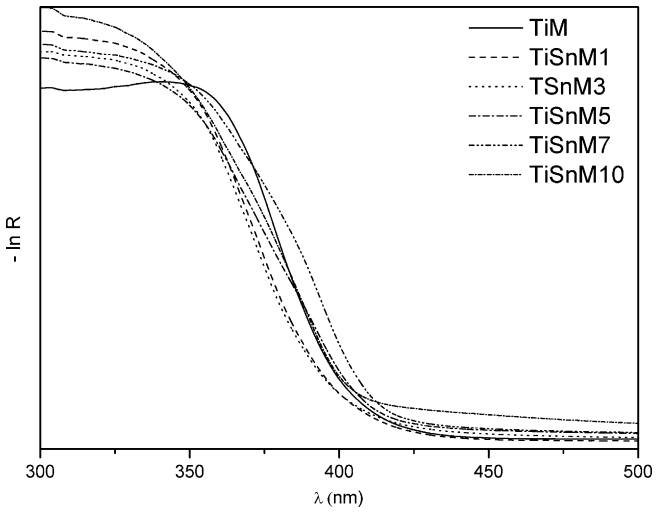

Fig. 4. Diffuse reflectance UV–vis spectra.

model [39]. This model considers nanoparticles as an intermediate case between a perfect infinite crystal and an amorphous material, in which a range of phonons around the centre of the Brillouin zone are involved in the Raman process, and explains the effect of crystal size on the position and width of the Raman lines [39,40]. Regarding the band widths, the expected trend of a higher width with decreasing crystal size is generally observed, although the sample with 1% Sn presents a lower width than that expected from the model. Apart from that, no higher deviation from the model is observed when introducing Sn^{4+}. In the case of the Raman shifts, only a value slightly lower than that expected from the phonon confinement model is observed for samples TiSnM5 and TiSnM7, contrarily to the rest of samples, which fit rather well the predicted trend. Therefore, this analysis does not clearly reveal an increment of structural defects on the anatase structure with the incorporation of Sn^{4+}, apart from those inherent to the reduced crystal size.

Fig. 4 shows the diffuse reflectance UV–vis spectra of the prepared samples. The band gap values estimated from these spectra are summarised in Table 1, considering both a direct and an indirect transition. TiO_2 is generally considered an indirect semiconductor, although some works have reported that, with crystal sizes of a few nanometres, direct transitions are observed in the spectra [30,45]. Assuming an error of ±0.05 eV in the calculation [30], no significant differences can be detected between the undoped reference and the doped samples. However, it must be noted that only the start of the absorption edge is considered for this calculation [30]. On the other hand, differences between the doped materials and the reference TiO_2 sample TiM can be observed in Fig. 4. In the case of the doped anatase samples, TiSnM1 and TiSnM3, the absorption edge is shifted to higher energy values with respect to TiM, which suggests electronic modifications of anatase due to the dopant cations. With the appearance of rutile, the initial part of the edge is shifted to lower energies with respect to the doped anatase samples, while the high energy part remains basically unchanged. This effect is clearly observed in the sample containing a higher amount of rutile, TiSnM7. This shift can be due to the fact that rutile presents a lower band gap energy than anatase [2], or it may be ascribed to a different effect of Sn^{4+} doping when the rutile phase is present. In the case of TiSnM10, an absorption tail in the visible part of the spectrum is observed. This can be related to the utilization of NH_3 in the synthesis procedure [46].

3.2. Photocatalytic activity

The photocatalytic degradation of trichloroethylene (TCE) was used as a test reaction to compare the activities of the synthesised photocatalysts. In the photocatalytic reactions, CO_2 and traces of phosgene were detected as gas-phase products, and after an induction period of ca. 15 min of irradiation in which conversions increased, steady values of TCE degradation rate were obtained. Fig. 5 shows the steady-state TCE degradation rates obtained with the different photocatalysts, expressed both per unit of mass of catalyst (Fig. 5A) and per unit of surface area (Fig. 5B). Eqs. (3) and (4) were employed for rate calculation:

$$r_{\text{mass}} = \frac{F(X_i - X_f)}{m\,K} \tag{3}$$

$$r_{\text{area}} = \frac{F(X_i - X_f)}{m\,S_{\text{BET}}K} \tag{4}$$

where F is the total flow rate (ml min^{-1}), X_i and X_f the mole fraction of TCE at the inlet and the outlet of the reaction, respectively, m the mass of catalyst (g), S_{BET} the BET surface area ($m^2\,g^{-1}$), and K = 60 s min^{-1} × 24.4 l mol^{-1} × 1000 ml l^{-1} at 298 K.

Fig. 5A shows that the rate values per mass of catalyst are higher, in general, on going from the undoped TiO_2 sample to the doped ones, with the maximum rate obtained with the sample TiSnM7. It should be noted that all the doped samples present higher BET areas than TiM (see Table 1), which is generally expected to increase photocatalytic activity. The higher surface area can be, nevertheless, regarded as an effect of tin doping, since, as it was discussed earlier, the presence of the guest cations has led to lower crystal sizes, and a good agreement is found between the trend of S_{BET} and that of crystal size. In any case, the activities displayed in Fig. 5A do not follow the same order as their BET surface areas. The best example of this is the case of sample TiSnM7

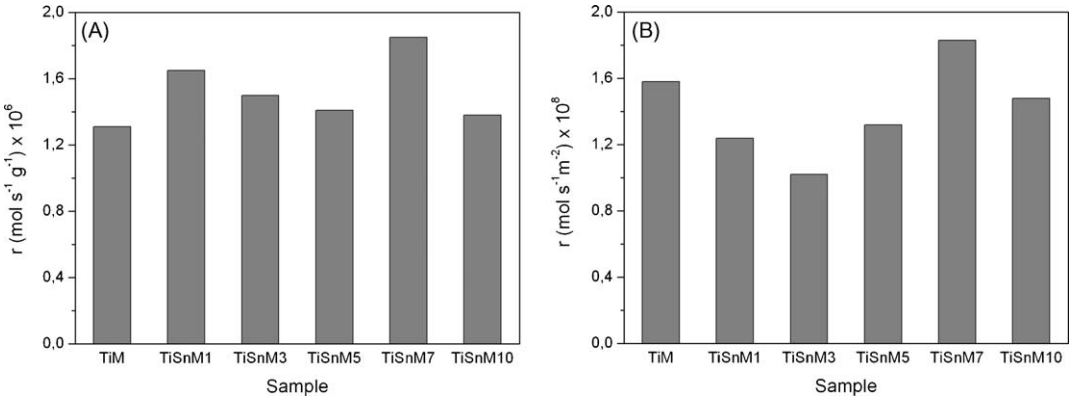

Fig. 5. Steady-state TCE degradation rates per unit of mass (A) and surface area (B) obtained with the different photocatalysts.

which, in spite of presenting a lower S_{BET} than the samples containing from 0 to 5% Sn, gives rise to the highest TCE degradation rate. This indicates that other factors apart from surface area influence the activity of the photocatalysts. In this respect, it is usually interesting to use reaction rates divided by the catalyst surface area, in order to eliminate the effect of this parameter and evaluate the intrinsic catalytic activity of the materials [47,48]. Regarding the degradation rates per unit of surface area (Fig. 5B), a different trend of photocatalytic activity with increasing Sn content is indeed observed. Firstly, the doped anatase samples (TiSnM1 and TiSnM3) led to a lower TCE degradation rate than undoped TiO_2. From these results, it can be deduced that tin doping of the anatase phase of TiO_2, with the employed synthesis procedure, is detrimental for the photocatalytic activity. This interpretation is reinforced by the fact that an increase of tin concentration in anatase, from TiSnM1 to TiSnM3, leads to a lower TCE degradation rate. However, a further increase in the doping level from TiSnM3 to TiSnM5, leads to a higher degradation rate. The difference is that, while TiSnM1 and TiSnM3 only contain the anatase phase, TiSnM5 also contains rutile. Indeed, an additional increase in the Sn^{4+} amount in TiSnM7 leads to both a higher rutile content and a higher TCE degradation rate, so that this sample presents a higher activity than the others shown in Fig. 5B, including the undoped TiO_2. The fact that photocatalytic activity increases with the presence of rutile, added to the detrimental effect of Sn^{4+} in the activity of anatase, lead us to conclude that the maximum activity observed in TiSnM7 benefits from the coexistence of both phases, caused by tin-doping, as mentioned earlier. The contacts between different semiconductor phases, with the adequate relative energies of the conduction and valence bands, can lead to a physical separation of the photogenerated charge carriers, reducing their recombination and, therefore, increasing photocatalytic activity. This charge separation has been observed in TiO_2(anatase)/TiO_2(rutile) composite photocatalysts and invoked to account for their high photocatalytic activities [49,50]. Therefore, the beneficial effect of Sn^{4+} in these samples appears to lie on the crystallisation of anatase and rutile in conditions in which undoped TiO_2 forms only the former phase, rather than on electronic modifications induced by the guest cations. On the other hand, for $Ti_{1-x}Sn_xO_2$ obtained by an organometallic-based synthesis route, we found that tin doping had other beneficial effects, in addition to the anatase–rutile contacts, giving rise to a very high photocatalytic activity [10,23]. This comparison reveals the importance of the preparation method of doped TiO_2 samples on their photocatalytic activity, making it difficult to draw general conclusions. Finally, a decrease in the reaction rate is observed from TiSnM7 to TiSnM10. According to the complexity of this sample, different factors can account for this observation. First, the rutile-to-anatase weight ratio in TiSnM10 is lower than that in TiSnM7, and the positive effect of anatase–rutile junctions may have been partially lost. On the other hand, the presence of the inactive SnO_2 phase, although found to be positive in certain configurations and conditions [7,20,21,51], may reduce the photocatalytic activity of the materials if there is not an adequate contact between TiO_2 and SnO_2 [7]. Finally, the modifications in the preparation method and the low crystallinity observed by XRD and Raman spectroscopy, must be also considered.

4. Conclusions

The microemulsion-mediated synthetic method presented here appears as a suitable way to prepare nanocrystalline $Ti_{1-x}Sn_xO_2$ photocatalysts with $0 < x < 0.10$. Tin-doped anatase is formed with $x < 0.05$, while both anatase and rutile phases crystallise when $x \geq 0.05$. In doped anatase–rutile samples, a preferential doping of rutile seems to occur. When $x = 0.10$, the synthetic procedure had to be slightly changed, and a TiO_2(anatase)/TiO_2(rutile)/SnO_2 phase mixture was formed. No significant modification of the band gap is found in any of the doped samples with respect to TiO_2, although slight modifications of the spectra are observed. Regarding photocatalytic activity for the gas phase degradation of trichloroethylene, no beneficial effect is observed for anatase samples with $x < 0.05$, apart from that due to the increased surface, while for samples with $0.05 \leq x < 0.10$, the beneficial effect of Sn^{4+} appears to be due to the formation of rutile, in addition to anatase, caused by the presence of tin.

Acknowledgement

This work has received financial support from the Spanish *Ministerio de Educación y Ciencia* (MEC), through the project CTQ2007-60480.

References

[1] M.R. Hoffmann, S.T. Martin, W. Choi, D.W. Bahnemann, Chem. Rev. 95 (1995) 69.
[2] O. Carp, C.L. Huisman, A. Reller, Prog. Solid State Chem. 32 (2004) 33.
[3] X. Chen, S.S. Mao, Chem. Rev. 107 (2007) 2891.
[4] M. Fernández-García, A. Martínez-Arias, J.C. Hanson, J.A. Rodríguez, Chem. Rev. 104 (2004) 4063.
[5] W. Choi, A. Termin, M.R. Hoffmann, J. Phys. Chem. B 98 (1994) 13669.
[6] P. Bouras, E. Stathatos, P. Lianos, Appl. Catal. B: Environ. 73 (2007) 51.
[7] D. Tudela, F. Fresno, J.M. Coronado, in: W. Chen (Ed.), Doped Nanomaterials andNanodevices, Vol. 3, American Scientific Publishers, Los Angeles, 2009, chapter 11, in press.
[8] J. Lin, J.C. Yu, D. Lo, S.K. Lam, J. Catal. 183 (1999) 368.
[9] A.I. Martínez, D.R. Acosta, G. Cedillo, Thin Solid Films 490 (2005) 118.
[10] F. Fresno, J.M. Coronado, D. Tudela, J. Soria, Appl. Catal. B: Environ. 55 (2005) 159.
[11] M.M. Oliveira, D.C. Schnitzler, A.J.G. Zarbin, Chem. Mater. 15 (2003) 1903.
[12] S. Mahanty, S. Roy, S. Sen, J. Cryst. Growth 261 (2004) 77.
[13] S.K. Zheng, T.M. Wang, W.C. Hao, R. Shen, Vacuum 65 (2002) 155.
[14] Y. Cao, W. Yang, W. Zhang, G. Liu, P. Yue, N. J. Chem. 28 (2004) 218.
[15] S.K. Kulshreshtha, R. Sasikala, V. Sudarsan, J. Mater. Chem. 11 (2001) 930.
[16] P.R. Santos, M.R. Cassia-Santos, L.G.P. Simoes, J.W. Gomes, E. Longo, J. Am. Ceram. Soc. 85 (2002) 282.
[17] L.B. Kong, J. Ma, H. Huang, J. Alloys Comp. 336 (2002) 315.
[18] J. Li, H.C. Zeng, J. Am. Chem. Soc. 129 (2007) 15839.
[19] J. Yu, S. Liu, M. Zhou, J. Phys. Chem. C 112 (2008) 2050.
[20] F. Fresno, D. Tudela, A.J. Maira, F. Rivera, J.M. Coronado, J. Soria, Appl. Organomet. Chem. 20 (2006) 220.
[21] F. Fresno, M.D. Hernández-Alonso, D. Tudela, J.M. Coronado, J. Soria, Appl. Catal. B: Environ. 84 (2008) 598.
[22] F. Fresno, C. Guillard, J.M. Coronado, J.M. Chovelon, D. Tudela, J. Soria, J.M. Herrmann, J. Photochem. Photobiol. A: Chem. 173 (2005) 13.
[23] F. Fresno, D. Tudela, J.M. Coronado, M. Fernández-García, A.B. Hungría, J. Soria, Phys. Chem. Chem. Phys. 8 (2006) 2421.
[24] S. Eriksson, U. Nylén, S. Rojas, M. Boutonnet, Appl. Catal. A: Gen. 265 (2004) 207.
[25] M. Wu, J. Long, A. Huang, Y. Luo, Langmuir 15 (1999) 8822.
[26] E. Stathatos, P. Lianos, F. Del Monte, D. Levy, D. Tsiourvas, Langmuir 13 (1997) 4295.
[27] A. Fuerte, M.D. Hernández-Alonso, A.J. Maira, A. Martínez-Arias, M. Fernández-García, J.C. Conesa, J. Soria, Chem. Commun. (2001) 2718.
[28] X.D. Zhou, W. Huebner, Appl. Phys. Lett. 79 (2001) 3512.
[29] H. Zhang, J.F. Banfield, J. Phys. Chem. B 104 (2000) 3481.
[30] N. Serpone, D. Lawless, R. Khairutdinov, J. Phys. Chem. 99 (1995) 16646.
[31] A.J. Maira, K.L. Yeung, C.Y. Lee, P.L. Yue, C.K. Chan, J. Catal. 192 (2000) 185.
[32] P.K. Nair, F. Mizukami, J. Nair, M. Salou, Y. Oosawa, H. Izutsu, K. Maeda, T. Okubo, Mater. Res. Bull. 33 (1998) 1495.
[33] K.-N.P. Kumar, K. Keizer, A.J. Burggraaf, T. Okubo, H. Nagamoto, J. Mater. Chem. 3 (1993) 923.
[34] J. Yang, D. Li, X. Wang, X. Yang, L. Lu, J. Solid State Chem. 165 (2002) 193.
[35] J. Liqiang, F. Honggang, W. Baiqi, W. Dejun, X. Baifu, L. Shudan, S. Jiazhong, Appl. Catal. B: Environ. 62 (2006) 282.
[36] H. Uchiyama, H. Imai, Chem. Commun. (2005) 6014.
[37] M. Fernández-García, A. Martínez-Arias, A. Fuerte, J.C. Conesa, J. Phys. Chem. B 109 (2005) 6075.
[38] L.E. Depero, L. Sangaletti, B. Allieri, E. Bontempi, A. Marino, M. Zocchi, J. Cryst. Growth 198/199 (1999) 516.
[39] S. Kelly, F.H. Pollak, M. Tomkiewicz, J. Phys. Chem. B 101 (1997) 2730.
[40] D. Bersani, P.P. Loticci, X.-Z. Ding, Appl. Phys. Lett. 72 (1998) 73.

[41] M. Gotic, M. Ivanda, S. Popovic, S. Music, A. Sekulic, A. Turkovic, K. Furic, J. Raman Spectrosc. 28 (1997) 555.
[42] G.A. Tompsett, G.A. Bowmaker, R.P. Cooney, J.B. Metson, K.A. Rodgers, J.M. Seakins, J. Raman Spectrosc. 26 (1995) 57.
[43] L. Abello, B. Bochu, A. Gaskov, S. Koudryavtseva, G. Lucazeau, M. Roumyantseva, J. Solid State Chem. 135 (1998) 78.
[44] W.F. Zhang, Y.L. He, M.S. Zhang, Z. Yin, Q. Chen, J. Phys. D: Appl. Phys. 33 (2000) 912.
[45] K.M. Reddy, S.V. Manorama, A.R. Reddy, Mater. Chem. Phys. 78 (2002) 239.
[46] I.N. Martyanov, S. Uma, S. Rodrigues, K.J. Klabunde, Chem. Commun. (2004) 2476.
[47] A.J. Maira, K.L. Yeung, J. Soria, J.M. Coronado, C. Belver, C.Y. Lee, V. Augugliaro, Appl. Catal. B: Environ. 29 (2001) 327.
[48] G. Marci, M. Addamo, V. Augugliaro, S. Coluccia, E. García-López, V. Loddo, G. Martra, L. Palmisano, M. Schiavello, J. Photochem. Photobiol. A: Chem. 160 (2003) 105.
[49] T. Kawahara, Y. Konishi, H. Tada, N. Toghe, J. Nishii, S. Ito, Angew. Chem. Int. Ed. 41 (2002) 2811.
[50] G. Li, K.A. Gray, Chem. Mater. 19 (2007) 1143.
[51] H. Tada, A. Hattori, Y. Tokihisa, K. Imai, N. Toghe, S. Ito, J. Phys. Chem. B 104 (2000) 4585.